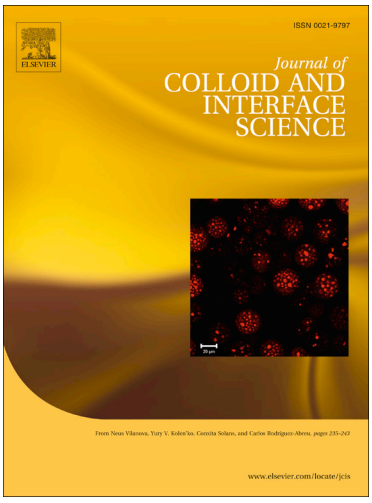

Regular Article

Enhanced visible light photocatalytic hydrogen evolution over porphyrin hybridized graphitic carbon nitride

Shunkang Mei, Jianping Gao, Ye Zhang, Jiangbing Yang, Yongli Wu, Xiaoxue Wang, Ruiru Zhao, Xiangang Zhai, Chaoyue Hao, Ruixia Li, Jing Yan

PII: S0021-9797(17)30797-X
DOI: http://dx.doi.org/10.1016/j.jcis.2017.07.030
Reference: YJCIS 22559

To appear in: *Journal of Colloid and Interface Science*

Received Date: 15 May 2017
Revised Date: 6 July 2017
Accepted Date: 8 July 2017

Please cite this article as: S. Mei, J. Gao, Y. Zhang, J. Yang, Y. Wu, X. Wang, R. Zhao, X. Zhai, C. Hao, R. Li, J. Yan, Enhanced visible light photocatalytic hydrogen evolution over porphyrin hybridized graphitic carbon nitride, *Journal of Colloid and Interface Science* (2017), doi: http://dx.doi.org/10.1016/j.jcis.2017.07.030

Enhanced visible light photocatalytic hydrogen evolution over porphyrin hybridized graphitic carbon nitride

Shunkang Mei[a], Jianping Gao[a,b], Ye Zhang[c], Jiangbing Yang[a], Yongli Wu[a], Xiaoxue Wang[a], Ruiru Zhao[a], Xiangang Zhai[a], Chaoyue Hao[a], Ruixia Li[a], Jing Yan[a,b,*]

* Corresponding Author.

[a] Department of Chemistry, School of Science, Tianjin University, Tianjin 300350, China.

[b] Collaborative Innovation Center of Chemical Science and Engineering (Tianjin), Tianjin 300072, China.

[c] Tianjin Textile Fibre Inspection Institute, Tianjin 300192, China

TEL: +8602227403475

E-mail address: jingyan@tju.edu.cn

Abstract

Tetra (4-carboxyphenyl) porphyrin (TCPP) was loaded on the surface of Pt/g-C_3N_4 via a simple adsorption process, and the microstructure and chemical structure of the composites were characterized by high resolution transmission electron microscopy, X-ray diffraction, X-ray photoelectron spectroscopy, Fourier transform infrared spectroscopy, UV-visible diffused reflectance spectroscopy and photoluminescence spectroscopy. Loading TCPP onto Pt/g-C_3N_4 enhanced the visible-light-driven photocatalytic evolution of H_2 from water. The TCPP/Pt/g-C_3N_4 composite with a TCPP loading of 1 wt % had the highest photoactivity, which was 2.1 times higher than that of Pt/g-C_3N_4. This improvement is attributed to enhanced visible light utilization by the TCPP/Pt/g-C_3N_4 resulting from the strong visible light response of TCPP. In addition, the formed organic heterostructure between TCPP and g-C_3N_4 with overlapping bad gaps accelerates the electron transfer and inhibits the recombination of the photogenerated electrons and holes on g-C_3N_4.

Keywords: Photocatalytic; Hydrogen production; g-C_3N_4; Porphyrin

1. Introduction

With the increasing consumption of fossil fuels which is exacerbating both the current energy crisis and environmental problems, the search for new clean and sustainable energy sources has become critical [1-2]. Hydrogen is a renewable and clean energy source which could help ease current energy problems [3]. Using solar radiation to split water is an easy and cost effective method to produce H_2 since solar energy is abundant and easily accessible [4-7].

Graphitic carbon nitride (g-C_3N_4) is a good photocatalyst to produce hydrogen, because it is inexpensive, non-toxic, non-polluting, and it has good thermodynamic

and chemical stability characteristics [8-11]. However, the photocatalytic activity of pure g-C_3N_4 is unsatisfactory under visible light irradiation [12]. Its low activity is due to three issues: (1) the band gap of g-C_3N_4 is 2.7 eV [13] with corresponds to an optical adsorption of 450 nm; this severely limits utilization of the visible-light in solar radiation; (2) g-C_3N_4 has a low electrical conductivity which results in fast recombination of photogenerated electron-hole pairs; (3) g-C_3N_4 has a small specific surface area. Three methods have been investigated to improve the photocatalytic performance of g-C_3N_4: the coupling of semiconductor photocatalysts [14-17], loading a noble metal as a co-catalyst [18-23] and dye sensitization [24,25].

Dye sensitization is a very effective way to enhance the photocatalytic performance of g-C_3N_4. Since dyes have good absorption in the visible region, they can greatly enhance the visible light utilization of g-C_3N_4 [26]. Moreover, most dyes can promote the transfer of electrons in visible-light-driven photocatalysis due to the heterostructures formed by the dyes and the g-C_3N_4 [27-28].

Porphyrin and its derivatives play a pivotal role in nature. For instance, chlorophyll is indispensable for the photosynthesis of green plants [29]. Inspired by this, porphyrin has been used in the photocatalytic production of hydrogen with some inspiring results [30-32]. Porphyrin is regarded as an appealing photosensitizer because of its great chemical stability and its large conjugated structure. Its large conjugated π-electron system endows porphyrin with a wide absorption band in the visible region and gives it excellent light-induced properties.

Several groups have reported promising results for porphyrin sensitization. For example, metal porphyrin modified TiO_2 shows good abilities for the photo-production of hydrogen and for the photodegradation of organic pollutants [33-35]. Reduced graphene oxide sheets and porphyrins have been combined through

π-π stacking to give strong interactions between the two conjugated system and this material exhibited outstanding photocatalytic hydrogen production [35]. Using the same mechanism, putting g-C_3N_4 and porphyrin together resulted in a superior photodegradation catalyst [27]. These noncovalent interactions between porphyrin molecules and photocatalysts are much easier to accomplish than covalent interactions since there are limited functional groups in g-C_3N_4 that can be modified. Further porphyrins can act as photosensitizers and light harvesters to generate electrons and holes. Since the porphyrin and photocatalyst form a heterostructure, the photogenerated electrons of the excited porphyrin can be efficiently transferred to the photocatalyst which enhances the photocatalytic performance [27, 33-36].

Inspired by these previous works, herein tetra (4-carboxyphenyl) porphyrin (TCPP), with a wide absorption band in the visible region and a band gap of 2.32 eV [37], was selected as a photosensitizer for g-C_3N_4. A series of TCPP sensitized photocatalysts were synthesized via a simple method and characterized by various instrumental techniques. The effect of the amount of TCPP loading on the catalytic performance was studied. The effects of TCPP on the absorption of visible light, on the transfer of photo-generated electrons and on hydrogen production were all studied. In addition, a possible reaction mechanism is proposed.

2. Experimental

2.1 Materials preparation

TCPP (97%) was purchased from Aladdin-reagent Co. Ltd., Shanghai, China. Melamine (99%) was purchased from J&K Scientific Ltd., Shanghai, China. All other chemicals were purchased from Tianjin Chemical Reagent Co. Ltd. All chemicals were used as received without further purification.

2.2 Sample preparation

2.2.1 Synthesis of g-C_3N_4

The g-C_3N_4 was prepared by heating melamine in a tube furnace. Typically, 3 g of melamine was placed in a sealed alumina crucible, heated to 550 °C at a heating rate of 10 °C min^{-1} and kept at this temperature for 4 h. The resulting light yellow product was collected and ground into powder using an agate mortar [38].

2.2.2 Synthesis of Pt/g-C_3N_4 composite

Pt nanoparticles were loaded onto the g-C_3N_4 surface via a simple in situ reduction procedure using an aqueous solution of $H_2PtCl_6 \cdot 6H_2O$ as a precursor. First, 0.5 g g-C_3N_4 was added to 50 mL deionized water and then ultrasonicated for 1 h. Then, 265.5 μL of 0.05 g mL^{-1} H_2PtCl_6 aqueous solution was slowly added into the resultant mixture. After 30 minutes of magnetic stirring, 5 mL of 0.5 M $NaBH_4$ solution was added dropwise over the course of 20 min and the solution was then magnetically stirred for 2 h. Finally, the product was separated by centrifugation, washed three times with deionized water and dried at 80 °C for 8 h (Scheme 1) [39].

2.2.3 Synthesis of TCPP/g-C_3N_4 composites

The TCPP/g-C_3N_4 composite was synthesized using the method previously reported in the literature [27]. First, 50 mg g-C_3N_4 powder was added to 10 mL of ethanol and then the mixture was ultrasonicated for 1 h. Next, 10 mL of TCPP ethanol solution (0.5 mg mL^{-1}) was slowly added to the above solution and the mixture was ultrasonicated for 1 h. The mixture was then continually stirred at 80 °C until the solvent was completely evaporated. Finally, the resulting product was dried overnight at 80 °C. TCPP/g-C_3N_4 composites with different TCPP ratios were prepared using the same procedure and adjusting the concentration of TCPP solution accordingly. The prepared composites were labeled as $TCPP_X$/g-C_3N_4, where X represents the proportion by weight of TCPP in the composites.

2.2.4 Synthesis of TCPP/Pt/g-C_3N_4 composites

A series of TCPP/Pt/g-C_3N_4 composites labeled as $TCPP_X$/Pt/g-C_3N_4 were synthesized using the same method as that for TCPP/g-C_3N_4 except g-C_3N_4 was replaced with the as-prepared Pt/g-C_3N_4 (Scheme 1).

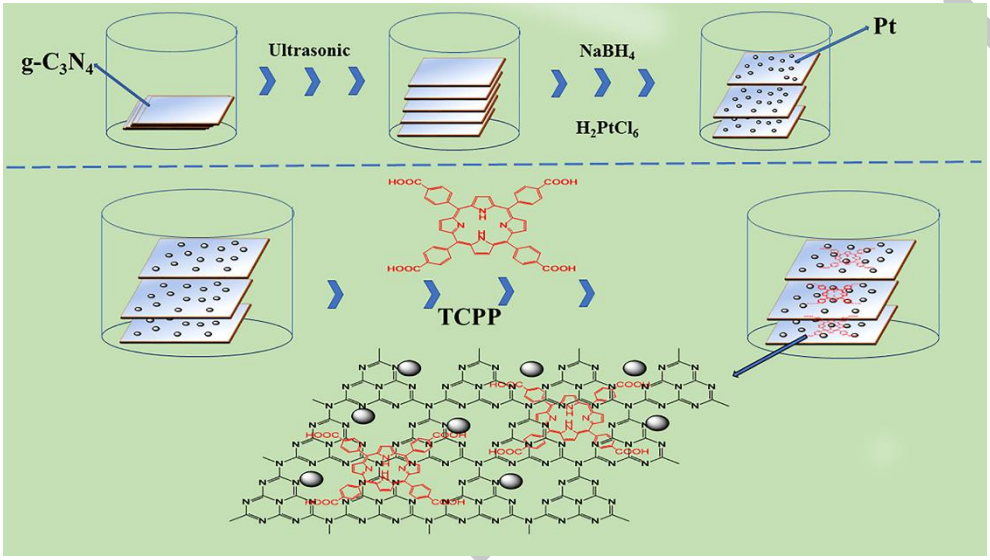

Scheme 1. Schematic illustration of the preparation of the $TCPP_X$/Pt/g-C_3N_4 composites.

2.3. Material characterization

The morphology and microstructure and energy dispersive X-ray spectroscopy (EDS) pattern of the as-prepared samples were characterized using transmission electron microscopy (TEM, Tecnai G2 F20). The crystal structure of the samples was determined using X-ray diffraction (XRD, D/MAX-2500, Japan) with a Cu Kα radiation source in the range of 10-80^o (2θ) with a scan rate at 10^o min^{-1}. X-ray photoelectron spectroscopy (XPS) with an Mg Kα anode (PHI1600 ESCA System, PERKIN ELMER, US) was used to determine the composition of the samples. Ultraviolet-visible (UV-Vis) diffuse reflectance spectroscopy (DRS) measurement of all composites were performed with a UV-Vis spectrophotometer (UV2450, Shimadzu,

Japan), using $BaSO_4$ as the reflectance standard. Fourier transform infrared (FTIR) spectra were collected on a Bruker Alpha FTIR in the region of 400-4000 cm^{-1} using KBr as a reference. Photoluminescence (PL) spectra were obtained on a Varian Cary Eclipse fluorescence spectrometer at room temperature with an excitation wavelength of 350 nm.

2.4. Photocatalytic H_2 production

The H_2 production experiments were carried out in a photocatalytic reactor (USA ACE GLASS, Vineland, NJ). Typically, 5 mL of 10 vol % triethanolamine (TEOA) aqueous solution (the electron donor) was added to a 10-mL quartz tube and saturated with N_2 for 30 minutes. Then 5 mg of catalyst was added and the solution was saturated with N_2 for another 5 mins to completely remove oxygen before irradiation. During the photocatalytic process, the solution was constantly stirred with a magnetic stirrer to ensure that the catalyst was fully exposed to the light. The light source was a Hg lamp (450 W) with a cut off filter ($\lambda > 380$ nm). During the entire reaction process, the system was maintained at 25 °C using flowing water. The amount of hydrogen produced was detected by gas chromatography (GC, CP 3800 Varian) using high purity N_2 as the carrier gas with a TDX-01 column.

3. Results and discussion

3.1. Materials and characterization

The morphology and microstructure of the prepared TCPP, g-C_3N_4, $TCPP_1$/g-C_3N_4, Pt/g-C_3N_4 and $TCPP_1$/Pt/g-C_3N_4 were first characterized by TEM and the results are shown in Fig. 1. The TCPP (Fig. 1a) is composed of lots of debris structures whereas g-C_3N_4 (Fig. 1b) has an aggregated structure composed of nanosheets. The micrograph of $TCPP_1$/g-C_3N_4 (Fig. 1c) shows that the TCPP was successfully loaded onto the surface of g-C_3N_4 and the images for the platinum

containing samples (Fig. 1d-e) show that Pt nanoparticles with an average particle size of about 4 nm were successfully loaded onto the surface of the g-C_3N_4 nanosheets. The image for $TCPP_1$/Pt/g-C_3N_4 (Fig. 1f) shows that both TCPP and Pt nanoparticles were deposited onto the surface of g-C_3N_4. EDS was also used to analyze $TCPP_1$/Pt/g-C_3N_4 (Fig. 1g) and the results show that the C: N atomic ratio in the red region of Fig. 1f was 5:4. This is higher than that for g-C_3N_4 (3:4). This also indicates that TCPP was successfully loaded onto g-C_3N_4. The weight ratio of Pt was about 1.1%. The TEM images demonstrate that a $TCPP_1$/Pt/g-C_3N_4 ternary heterostructure was successfully synthesized. The interactions among the TCPP, Pt and g-C_3N_4 may accelerate electron transfers within the material [24].

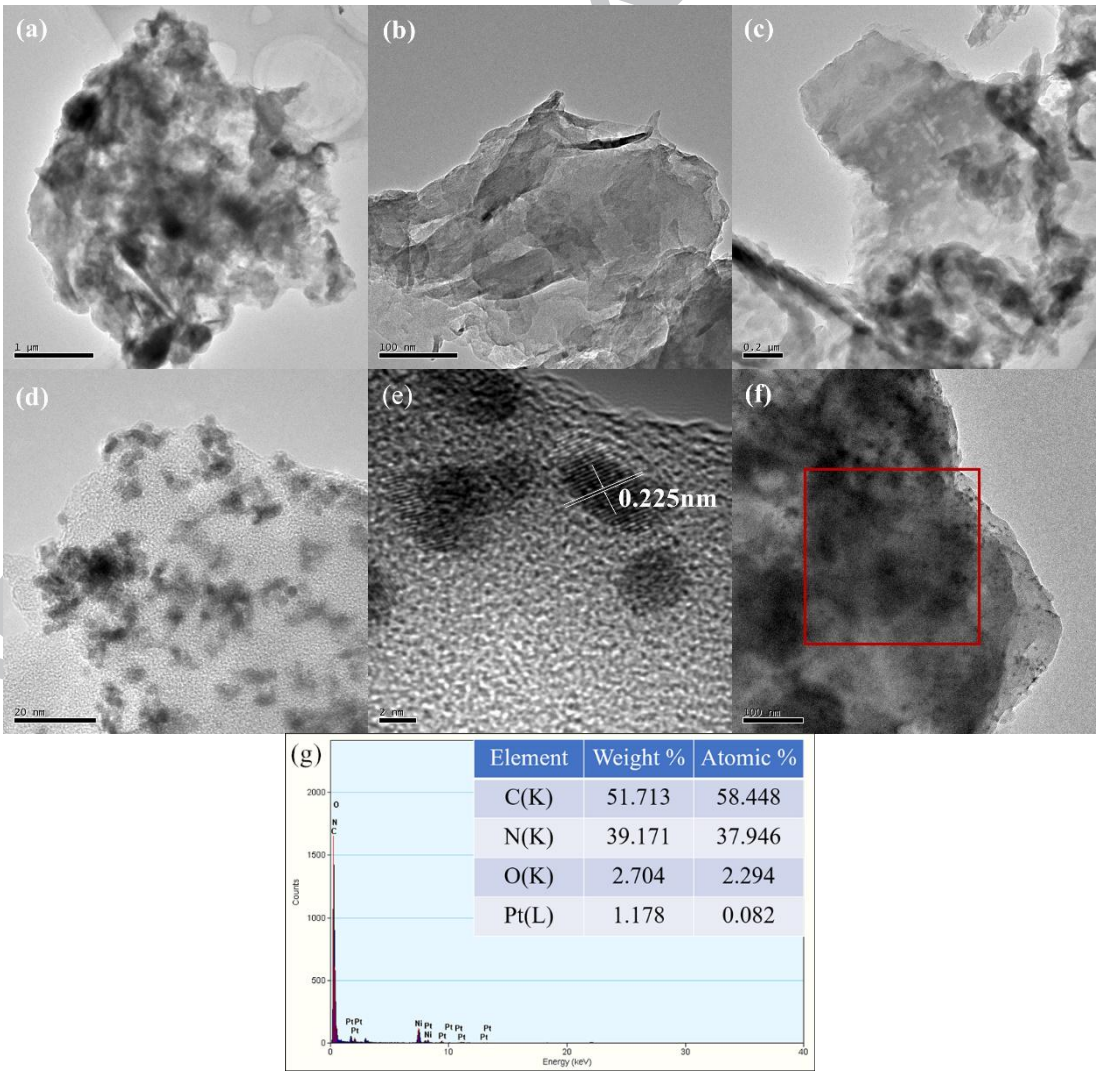

Fig. 1.TEM images of (a) pure TCPP; (b) pure g-C_3N_4; (c) $TCPP_1$/g-C_3N_4; (d, e) Pt/

g-C_3N_4;(f) $TCPP_1$/Pt/g-C_3N_4;(g) EDS of $TCPP_1$/Pt/g-C_3N_4(red area in Fig. f)

The crystal structures of the samples were studied by XRD and the results are shown in Fig. 2. The g-C_3N_4 pattern has two distinct peaks at 13.0° and 27.4°, which correspond to the g-C_3N_4 (002) and (100) crystal planes respectively [40]. The TCPP pattern exhibits a very wide diffraction peak centered at about 20.9°. In the $TCPP_1$/g-C_3N_4 pattern, a peak for TCPP is not observed which is due to the low TCPP content. The Pt/g-C_3N_4 spectrum contains two additional diffraction peaks at 39.8° and 46.1° which correspond respectively to the (111) and (200) planes of the Pt nanoparticles [40]. Similarly, in the in $TCPP_1$/Pt/g-C_3N_4 pattern, only the diffraction peaks of g-C_3N_4 and Pt are found. All the g-C_3N_4-containg samples have similar XRD patterns indicating that the overall structures of the samples are similar and so the addition of TCPP and Pt has no effect on the crystal structure of g-C_3N_4.

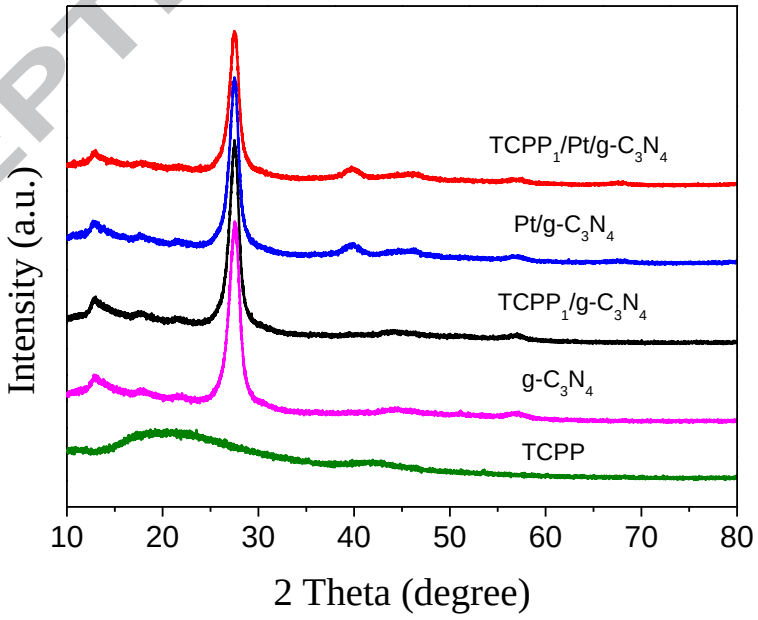

Fig. 2. XRD patterns of TCPP, g-C_3N_4, $TCPP_1$/g-C_3N_4, Pt/g-C_3N_4 and $TCPP_1$/Pt/g-C_3N_4

XPS was used to characterize the composition and chemical states of $TCPP_1/Pt/g\text{-}C_3N_4$. The XPS spectrum is shown in Fig. 3a and the C 1s spectrum is shown in Fig. 3b. The peak at 284.8 eV corresponds to C-C and/or C= C, whereas the peak at 287.8 eV can be assigned to N-C=N [21]. The N1S binding energy region in Fig. 3c contains three peaks. The peak at 398.3 eV can be assigned to sp^2-hybridized aromatic N atoms which are bonded to C atoms (C-N=C), the peak centered at 400.6 eV is due to tertiary N atoms bonded to C atoms in the form of $N–(C)_3$ and the weak peak at 403.5 eV originates from N atoms bonded to three C atoms in the aromatic rings [28]. Figure 3b shows the Pt 4f spectrum in which the peaks at 70.1 and 76.6 eV are from metallic Pt (Pt (0)), whereas the peak at 73.3 eV is from Pt^{2+} [18]. The O 1s spectrum is shown in Fig. 3e and the peak at 532.4 eV can be attributed to -OH groups [18].

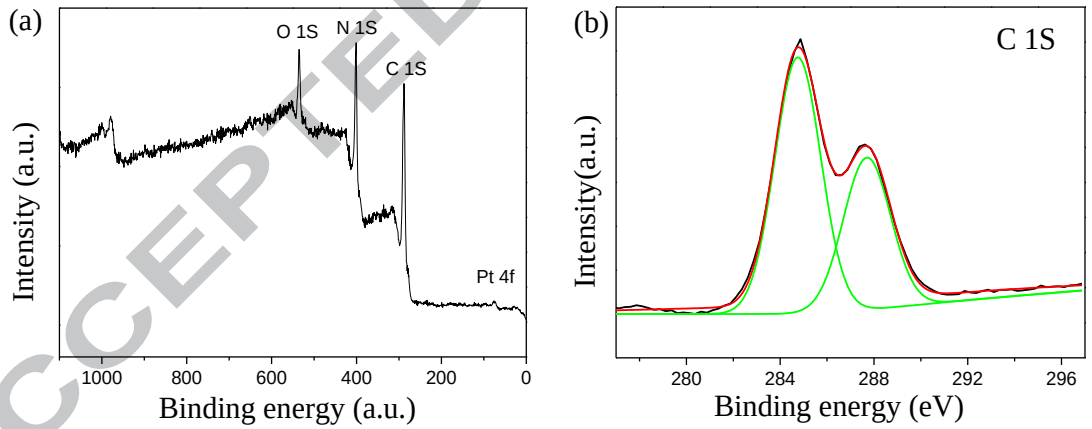

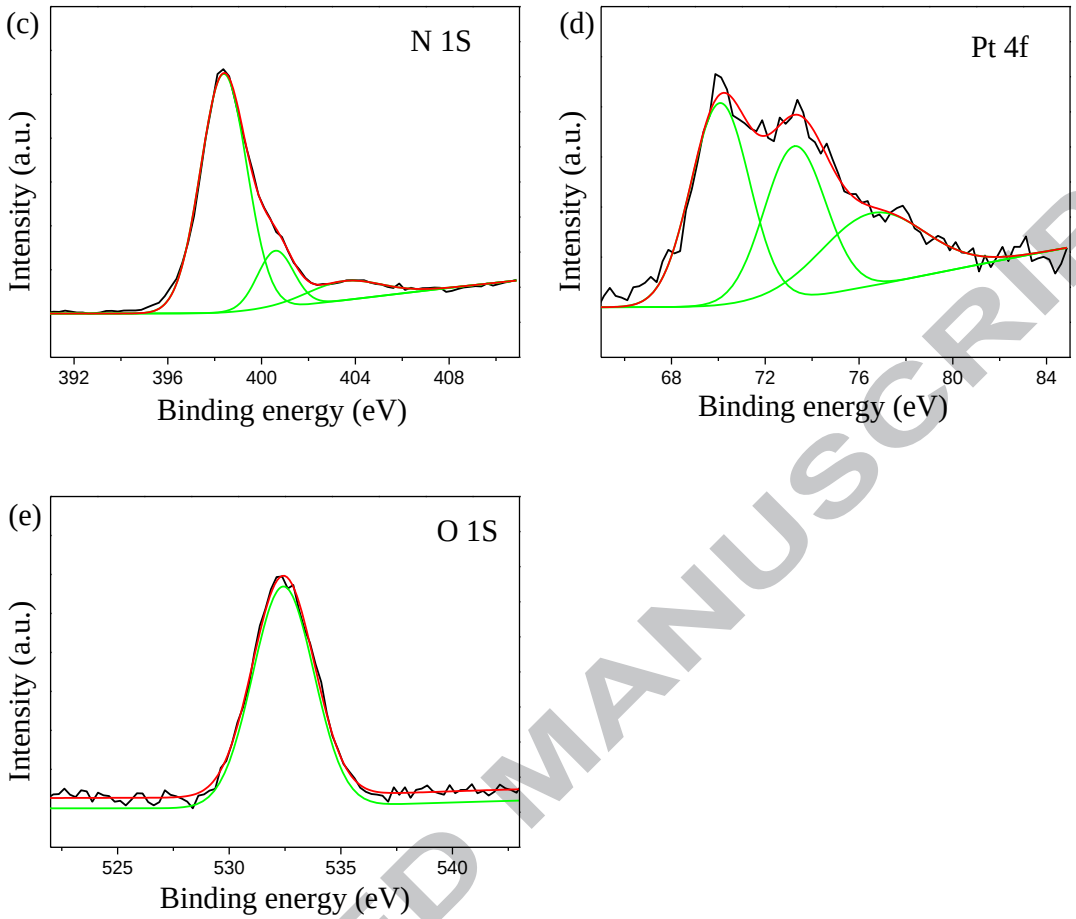

Fig. 3. XPS spectra of (a) $TCPP_1/Pt/g\text{-}C_3N_4$ composite and high-resolution XPS spectra of (b) C 1s, (c) N 1s, (d) Pt 4f, and (e) O 1s binding energy regions.

The structures of the synthesized composites were further characterized by FTIR spectroscopy and the results are shown in Fig. 4. Figure 4a shows the FTIR spectra of $g\text{-}C_3N_4$, TCPP, $TCPP_1/g\text{-}C_3N_4$, $Pt/g\text{-}C_3N_4$ and $TCPP_1/Pt/g\text{-}C_3N_4$. In the spectrum of the pristine $g\text{-}C_3N_4$, a wide band is observed at 3000-3500 cm^{-1} which primarily corresponds to the N-H stretching vibrations. The bands in the region from 1200 to 1650 cm^{-1} (1639, 1562, 1408, 1321 and 1239 cm^{-1}) are associated with C-N and C=N stretching vibrations. The sharp band at 807 cm^{-1} is related to out-of-plane bending vibrations which are characteristic of heptazine rings [15, 41]. The spectra of

$TCPP_1/g\text{-}C_3N_4$, $Pt/g\text{-}C_3N_4$ and $TCPP_1/Pt/g\text{-}C_3N_4$ are all similar to that of $g\text{-}C_3N_4$, again indicating that TCPP and Pt have no effect on the structure of $g\text{-}C_3N_4$.

The FT-IR spectra of a series of $TCPP_X/g\text{-}C_3N_4$ composites are shown in Fig. 4b. The $TCPP/g\text{-}C_3N_4$ composites all have the same characteristic peaks and no peaks characteristic of TCPP are seen which is due to the low content of TCPP. This may indicate that TCPP is loaded on $g\text{-}C_3N_4$ through non-covalent bonds rather than via covalent bonds [27]

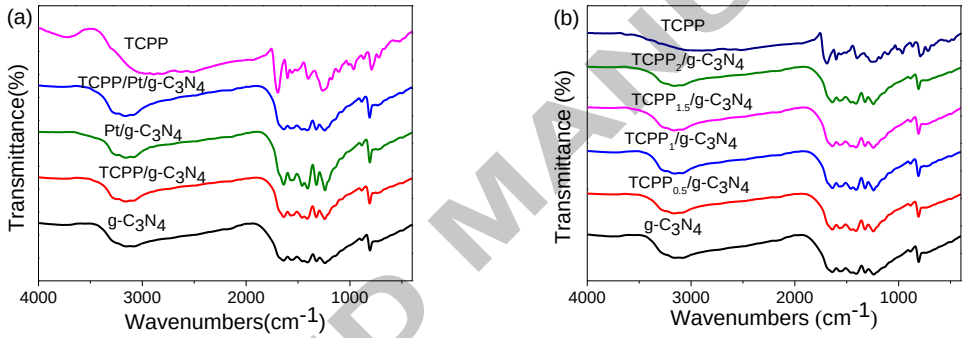

Fig. 4. FTIR spectra of (a) $g\text{-}C_3N_4$, TCPP, $TCPP_1/g\text{-}C_3N_4$, $Pt/g\text{-}C_3N_4$ and $TCPP_1/Pt/g\text{-}C_3N_4$ and (b) a series of $TCPP_X/g\text{-}C_3N_4$ composites

UV–Vis diffuse reflection spectroscopy is a common and effective method to accurately characterize the light absorbing abilities of material. Figure 5 shows the UV absorption spectra of $g\text{-}C_3N_4$, $Pt/g\text{-}C_3N_4$, $TCPP_1/g\text{-}C_3N_4$, $TCPP_1/Pt/g\text{-}C_3N_4$ and TCPP. The band gap for $g\text{-}C_3N_4$ is 2.7 eV, and as the UV-vis spectra shows, $g\text{-}C_3N_4$ does not absorb visible light at $\lambda > 450$ nm. In contrast, TCPP absorbs throughout the visible region. It has an intense absorption peak at 430 nm and four weak absorption peaks in the range of 500-700 nm. These peaks correspond to the Soret band and the four Q porphyrin bands, respectively. The absorption spectrum of $Pt/g\text{-}C_3N_4$ is basically the same as that for $g\text{-}C_3N_4$, indicating that Pt has no effect on the

absorbance of g-C_3N_4. The absorption spectra of $TCPP_1$/g-C_3N_4 and $TCPP_1$/Pt/g-C_3N_4 are combinations of those for g-C_3N_4 and TCPP. However, compared with pure TCPP, the Soret band in $TCPP_1$/Pt/g-C_3N_4 shifted from 416 nm to 430 nm and the Q1 band shifted from 512 nm to 524 nm. This red shift is due to π-π stacking [36]. This phenomenon shows that the TCPP and g-C_3N_4 are not just physically mixed but that they have formed a heterogeneous structure.

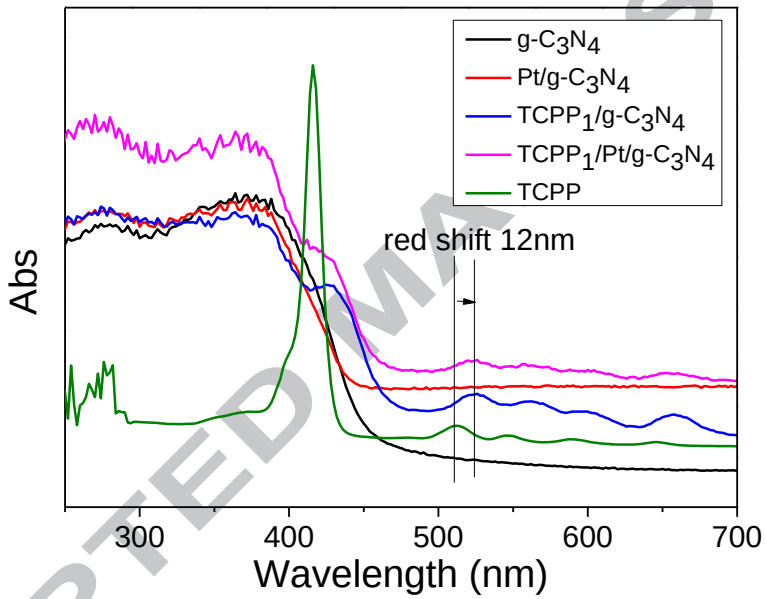

Fig. 5. UV–Vis diffuse reflection spectra of g-C_3N_4, Pt/g-C_3N_4, $TCPP_1$/g-C_3N_4, $TCPP_1$/Pt/g-C_3N_4 and TCPP.

3.2. Photocatalytic H_2 production

The photocatalytic H_2 production activities of the samples were evaluated under visible light irradiation (λ > 380 nm), using 10 vol % TEOA aqueous solution as an electron donor, and the results are shown in Fig. 6a. The photocatalytic H_2 evolution rate for pure g-C_3N_4 is very low (only about 6 μmol g^{-1} h^{-1}). The H_2 evolution rates for $TCPP_1$/g-C_3N_4 and Pt/g-C_3N_4 reached 30 and 564 μmol g^{-1} h^{-1} respectively. The higher

activities are because both TCPP and Pt improve photoinduced electron transfers and inhibit recombination of photogenerated electron-hole pairs in g-C_3N_4 [39]. The H_2 evolution rate of the $TCPP_1$/Pt/g-C_3N_4 composite (1208μmol g^{-1} h^{-1}) is 2.1 times higher than that of Pt/g-C_3N_4. In this ternary composite, both TCPP and Pt nanoparticles can inhibit the recombination of photogenerated electron-hole pairs and TCPP also significantly improves the ability of g-C_3N_4 to absorb visible light [27]. The synergistic effect of Pt nanoparticles and TCPP plays an important role in improving the g-C_3N_4 photocatalytic activity.

The effect of the amount of loaded TCPP on the photocatalytic activity of $TCPP_X$/Pt/g-C_3N_4 was studied and the results are shown in Fig. 6b. With the increase of TCPP content, the H_2 production rate was improved and highest H_2 production rate was achieved with a TCPP loading of 1 wt %. Further increasing TCPP resulted in lower H_2 production rates. This may be because excess TCPP causes a decrease in the number of active sites [25].

The stability of the catalyst is a critical factor in assessing whether the catalyst can be used in production. The $TCPP_1$/Pt/g-C_3N_4 catalyst was used for H_2 production for five cycles (25 h) and the result are shown in Fig. 6c. After five cycles, the catalyst retained 90% of its initial activity, indicating that the catalysts exhibit excellent stability under visible light irradiation. A possible reason for the loss in catalytic activity may be that a few of the TCPP molecules were desorbed from the g-C_3N_4 nanosheets during the continuous agitation process. Overall, the $TCPP_1$/Pt/g-C_3N_4 ternary composite catalyst exhibits a remarkable recycling capability.

The photocatalytic H_2 production performance of photocatalysts is also affected by various electron donors [42]. The effects of methanol, ascorbic acid (AA), ethylenediaminetetraacetic acid (EDTA) and TEOA on the photocatalytic

performance of $TCPP_1/Pt/g\text{-}C_3N_4$ were studied and the results are shown in Fig. 6d. TEOA is the best electron donor for the catalyst and methanol is the worst. This remarkable difference may be due to the differences in the oxidation-reduction potentials of the electron donors [43].

The concentration of H^+ is another factor that influences H_2 evolution. So the photocatalytic performance of $TCPP_1/Pt/g\text{-}C_3N_4$ at different pH values was investigated and the results are shown in Fig. 6e. The best photocatalytic performance was obtained at pH 9. The lower performances at more acidic conditions are due to the protonation of TEOA. The lower H_2 evolution rate at higher pH values is mainly due to the decrease of H^+ concentration [44].

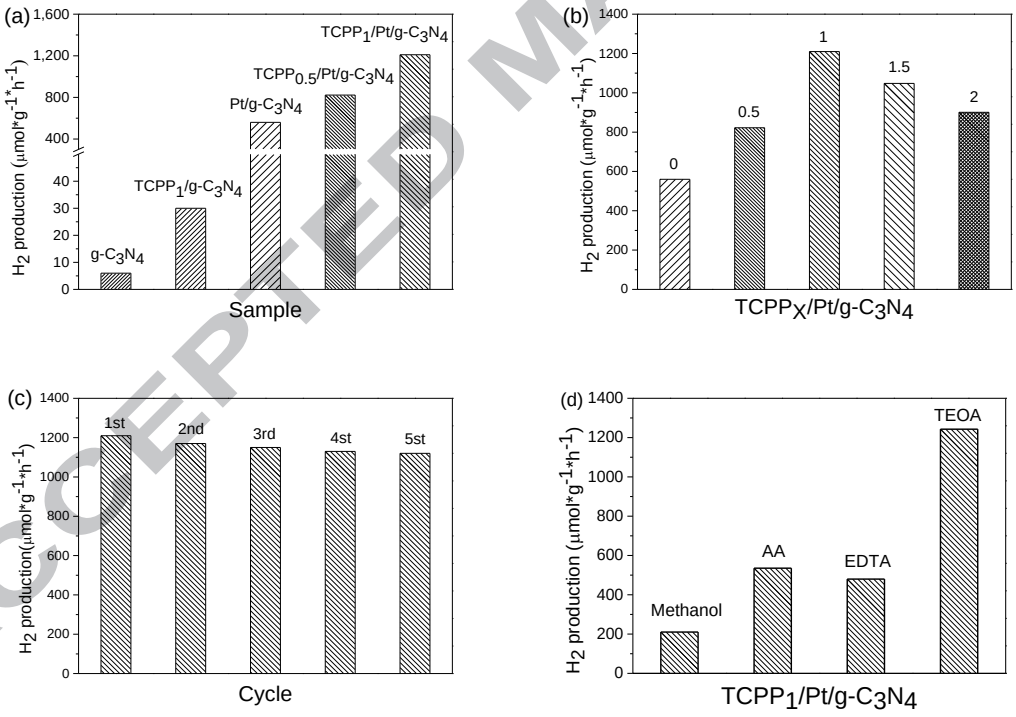

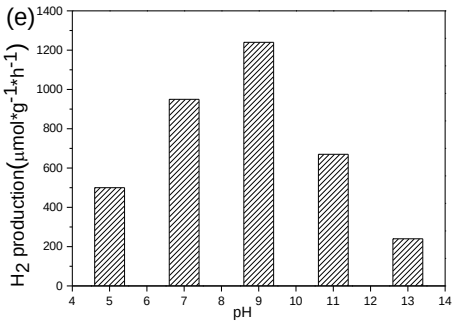

Fig. 6. Under visible-light irradiation, (a) rate of photocatalytic H_2 production by photocatalysts; (b) rate of photocatalytic H_2 production by $TCPP_X/Pt/g\text{-}C_3N_4$ with different TCPP mass ratios (0, 0.5, 1.0, 1.5 and 2 wt %); (c) reusability of the $TCPP_1/Pt/g\text{-}C_3N_4$ photocatalyst; (d) Effects of different electron donors (methanol, ascorbic acid, EDTA, TEOA) on the photocatalytic performance of $TCPP_1/Pt/g\text{-}C_3N_4$; (e) Effect of pH on photocatalytic performance of $TCPP_1/Pt/g\text{-}C_3N_4$.

3.3. Proposed mechanism

A possible mechanism for the electron transfer in the photocatalytic process is shown in Fig. 7. Based on the UV-vis diffuse reflectance data, the bandgap energies of $g\text{-}C_3N_4$ and TCPP are 2.7 and 2.5 eV, respectively (Fig S1a and S1b). According to previous reports, TCPP is a photosensitizer with a HOMO at +0.96 eV vs. normal hydrogen electrode (NHE) [37]; whereas the redox potentials of the conduction band (CB) and the valence band (VB) of $g\text{-}C_3N_4$ are at -1.3 and +1.4 eV vs. NHE respectively [13]. As shown in Fig. 7, both TCPP and $g\text{-}C_3N_4$ can be excited by absorbing visible light (λ> 380 nm). The electrons are excited to the LUMO and CB, forming holes in the HOMO and VB. Since the LUMO of TCPP is more negative than the CB of $g\text{-}C_3N_4$, the photogenerated electrons can be transferred from the LUMO of TCPP to the CB of $g\text{-}C_3N_4$. Due to the surface plasmon resonance effect of the Pt nanoparticles, the electrons accumulated in the $g\text{-}C_3N_4$ CB can then be captured by the

Pt nanoparticles, which provide reaction sites, so the reduction of H^+ to H_2 is easy to achieve [24]. Concurrently, the VB of g-C_3N_4 is more positive than the HOMO of TCPP, so the holes of g-C_3N_4 are transferred to the HOMO of TCPP [27]. At the same time, the photogenerated holes in TCPP and g-C_3N_4 are filled with electrons from the electron donor, TEOA. Thus, an effective and fast electron separation is achieved. This rapid and efficient electron separation suppresses the recombination of the photogenerated electron holes, thereby improving the photocatalytic performance under visible light irradiation.

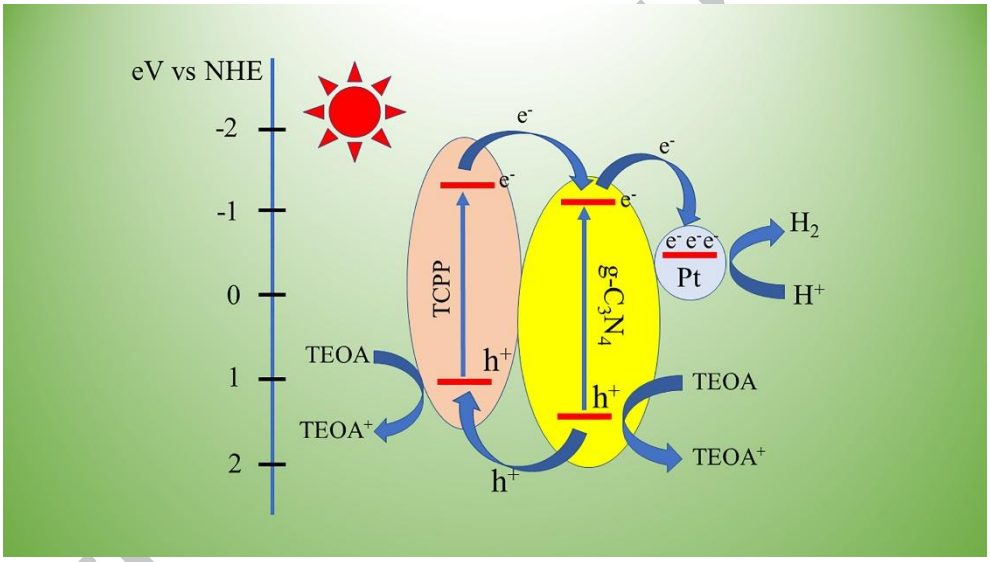

Fig. 7. Proposed mechanism for photocatalytic H_2 evolution over TCPP/Pt/g-C_3N_4 under visible-light irradiation (λ >380 nm).

To verify the mechanism, photoluminescence spectra were used to study the photogenerated electron-hole pair transfer and recombination processes. Figure 8a shows the PL spectra for g-C_3N_4, $TCPP_1$/g-C_3N_4, Pt/g-C_3N_4 and $TCPP_1$/Pt/g-C_3N_4 at an excitation wavelength of 350 nm. The PL spectrum of g-C_3N_4 exhibits a broad intense emission peak. The intensities of the emission peaks in $TCPP_1$/g-C_3N_4, Pt/g-C_3N_4 and $TCPP_1$/Pt/g-C_3N_4 are significantly weaker than that in g-C_3N_4. This

clearly demonstrates that both Pt and TCPP inhibit the recombination of the photogenerated electrons and holes in g-C_3N_4. The emission intensity is the lowest for $TCPP_1$/Pt/g-C_3N_4 which indicates that Pt and TCPP may have a synergistic effect on the charge transfer. In addition to the lower intensities, there are also red shifts in the emission peaks of $TCPP_1$/g-C_3N_4 and $TCPP_1$/Pt/g-C_3N_4. This also indicates that there are interactions between g-C_3N_4 and TCPP [27]. Thus it can be concluded that TCPP and g-C_3N_4 form a heterogeneous structure.

The PL spectra for $TCPP_X$/g-C_3N_4 are shown in Fig. 8b. With the increase of TCPP content, the fluorescence intensity decreased. $TCPP_1$/g-C_3N_4 has the weakest PL peak. To further improve the TCPP content, PL response becomes stronger. This phenomenon may be due to the presence of excessive TCPP which reduces the reduction of active sites for H_2 production [25].

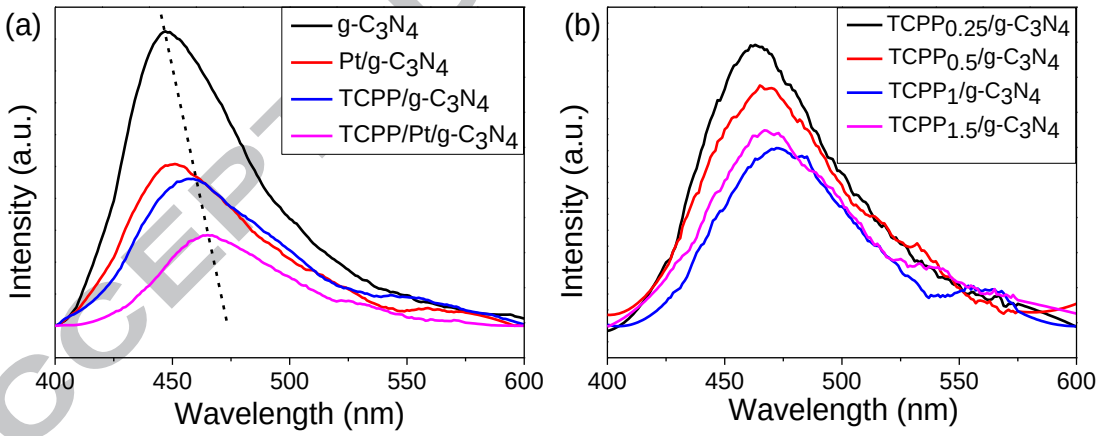

Fig. 8. Photoluminescence spectra of: (a) g-C_3N_4, $TCPP_1$/g-C_3N_4, Pt/g-C_3N_4 and $TCPP_1$/Pt/g-C_3N_4 and (b) $TCPP_{0.25}$/g-C_3N_4, $TCPP_{0.5}$/g-C_3N_4, $TCPP_1$/g-C_3N_4 and $TCPP_{1.5}$/g-C_3N_4.

4. Conclusions

In summary, a TCPP/Pt/g-C_3N_4 ternary composite photocatalyst for photocatalytic H_2 production was synthesized via a facile method. The catalyst has a high photocatalytic

activity under visible light irradiation. It not only has excellent hydrogen production efficiency but also exhibits good reusability. The catalyst with a TCPP content of 1 wt % had the highest photocatalytic H_2 production rate (1208 μmol g^{-1} h^{-1}) which was 2.1 times greater than that of Pt/g-C_3N_4. The TCPP and Pt play a synergistic role in improving the catalytic activity. The TCPP improved the ability of g-C_3N_4 to use visible light. In addition the co-catalyst Pt nanoparticles and the heterostructure formed by the TCPP and g-C_3N_4 via π-π stacking accelerated the electron transfer and inhibited the recombination of the photogenerated electrons and holes in g-C_3N_4. Compared to many previous reports of inorganic heterojunctions, this study provides a new way to construct organic heterojunctions for photocatalytic hydrogen production.

Acknowledgments

This work was supported by the National Science Foundation of China (51573126).

References

[1] A.J. Esswein, D.G. Nocera, Chem. Rev. 107 (2007) 4022-4047.

[2] S. Berardi, S. Drouet, L. Francàs, C. Gimbert-Suriñach, M. Guttentag, C. Richmond, T. Stoll, A. Llobet, Chem. Soc. Rev.43 (2014) 7501-7519.

[3] X.B. Chen, S. H. Shen, L.J. Guo, S. S. Mao, Chem. Rev. 110 (2010) 6503-6570.

[4] A. Kubacka, M. Fernandez-Garcia, G. Colon, Chem. Rev.112 (2012) 1555-1614.

[5] Q. Li, B.D. Guo, J.G. Yu, J.R. Ran, B.H. Zhang, H.J. Yan, J.R. Gong, J. Am. Chem. Soc. 133 (2011) 10878-10884.

[6] Y.Q. Qu, X.F. Duan, Chem. Soc. Rev.42(2013) 2568-2580.

[7] P.V. Kamat, J. Phys. Chem. C 111(2007) 2834-2860.

[8] C.C. Han, Y. Lu, J.L. Zhang, L. Ge, Y.J. Li, C.F. Chen, Y.J. Xin, L.N. Wu, S.M. Fang, J. Mater. Chem. A 3 (2015) 23274-23282

[9] Z.W. Zhao, Y.J. Sun, F. Dong, Nanoscale. 7 (2015) 15-37.

[10] D.J. Martin, P.J.T. Reardon, S.J.A. Moniz, J.W. Tang, J. Am. Chem. Soc. 136 (2014) 12568-12571.

[11] X.C. Wang, K. Maeda, A. Thomas, K. Takanabe, G. Xin, J.M. Carlsson, K. Domen, M. Antonietti, Nat. Mater.8 (2009) 76-80.

[12] J. Chen, S.H. Shen, P.H. Guo, M. Wang, P. Wu, X.X. Wang, L.J. Guo, Appl. Catal. B: Environ.152-153 (2014) 335-341.

[13] S. Chu, Y. Wang, Y. Guo, J.Y. Feng, C.C. Wang, W.J. Luo, X.X. Fan, Z.G. Zou, Catal. 3 (2013) 912-919.

[14] S.W. Cao, Y.P. Yuan, J. Fang, M.M. Shahjamali, F.Y.C. Boey, J. Barber, S.C.J. Loo, C. Xue, Int. J. Hydrogen Energ.38 (2013) 1258-1266.

[15] J.X. Wang, J. Huang, H.L. Xie, A.L. Qu, Int. J. Hydrogen Energ. 39 (2014) 6354-6363.

[16] B. Chai, T.Y. Peng, J. Mao, K. Lia, L. Zan, Phys. Chem. Chem. Phys.14 (2012) 16745-16752.

[17] Z.D. Gao, Y.F. Qu, X.M. Zhou, L. Wang, Y.Y. Song, P. Schmuki, Chemistryopen 5 (2016) 197-200.

[18] K.X. Lia, Z.X. Zeng, L.S. Yan, S.L. Luo, X.B. Luo, M.X. Huo, Y.H. Guo, Appl. Catal. B: Environ.165 (2015) 428-437.

[19] X.G. Li, W.T. Bi, L. Zhang, S. Tao, W.S. Chu, Q. Zhang, Y. Luo, C.Z. Wu, Y. Xie, Adv. Mater. 28 (2016) 2427-2431.

[20] X.H. Li, X.C. Wang, M. Antonietti, Chem. Sci. 3 (2012) 2170-2174.

[21] Y.F. Li, L. Fang, R.X. Jin, Y. Yang, X. Fang, Y. Xing, S.Y. Song, Nanoscale.7 (2015) 758-764.

[22] Y. Shiraishi, Y. Kofuji, S. Kanazawa, H. Sakamoto, S. Ichikawa, S. Tanakac, T. Hirai, Chem. Commun. 50 (2014) 15255-15258.

[23] J.J. Xue, S.S. Ma, Y.M. Zhou, Z.W. Zhang, M. He, ACS Appl. Mater. Inter. (2015) 7 9630-9637.

[24] J.Y. Qin, J.P. Huo, P.Y. Zhang, J. Zeng, T.T. Wang, H. P. Zeng, Nanoscale. 8 (2016) 2249-2259.

[25] Y.Y. Guo, S.S. Song, Y. Zheng, R.J. Li, T.Y. Peng, Dalton Trans.45 (2016) 14071-14079.

[26] S. Chen, C. Wang, B.R. Bunesc, Y.X. Lia, C.Y. Wang, L. Zang, Appl. Catal. A: Gen.498 (2015) 63-68.

[27] D.M. Chen, K.W. Wang, W.Z. Hong, R.L. Zong, W.Q. Yao, Y.F. Zhu, Appl. Catal. B: Environ. 166-167 (2015) 366-373.

[28] D.H. Wang, J.N. Pan, H.H. Li, J.J. Liu, Y.B. Wang, L.T. Kang, J.N. Yao, J. Mater. Chem. A 4 (2016) 290-296.

[29] E. Koposova, X. Liu, A. Pendin, B. Thiele, G. Shumilova, Y. Ermolenko, A. Offenhäusser, Y. Mourzina, J. Phys. Chem. C 120 (2016) 13873-13890.

[30] M.A. Fodor, O. Horváth, L. Fodor, G. Grampp, A. Wankmüller, Inorg. Chem. Commun.50 (2014) 110-112.

[31] M.M. Maitani, C.H. Zhan, D. Mochizuki, E. Suzuki, Y. Wada, Appl. Catal. B: Environ.147 (2014) 770-778.

[32] L. Mintrop, J. Windisch, C. Gotzmann, R. Alberto, B. Probst, P. Kurz, J. Phys. Chem. B119 (2015) 13698-13706.

[33] S. Afzal, W.A. Daoud, S.J. Langford, ACS Appl. Mater. Inter.5 (2013) 4753-4759.

[34] L. Gomathi Devi, M.L. ArunaKumari, Appl. Surf. Sci. 276 (2013) 521- 528.

[35] B.H. Yao, C. Peng, W. Zhang, Q.K. Zhang, J.F. Niu, J. Zhao, Appl. Catal. B: Environ. 174-175 (2015) 77-84.

[36] M.S. Zhu, Z. Li, B. Xiao, Y.T. Lu, Y.K. Du, P. Yang, X.M. Wang, ACS Appl. Mater. Inter. 5 (2013) 1732-1740.

[37] A. Kathiravan, R. Renganathan, J. Colloid Interface Sci. 331 (2009) 401-407.

[38] J. Zeng, T. Song, M.X. Lv, T.T. Wang, J.Y. Qin, H.P. Zeng, RSC Adv.6 (2016) 54964-54975.

[39] F. Fina, H. Mènard, J.T.S. Irvine, Phys. Chem. Chem. Phys. 17 (2015) 13929-13936.

[40] W.J. Ong, L.L. Tan, S.P. Chai, S.T. Yong, Dalton Trans.44 (2015) 1249-1257.

[41] Z.H. Hong, B. Shen, Y.L. Chen, B.Z. Lin, B.F. Gao, J. Mater. Chem. A 1 (2013) 11754-11761.

[42] Z. Jin, X. Zhang, Y. Li, S. Li, G. Lu, Catal. Commun.8 (2007) 1267-1273.

[43] X.H. Zhang, L.J. Yu, C.S. Zhuang, T.Y. Peng, R.J. Li, X.G. Li, ACS Catal.4(2014) 162-170.

[44] Z. Li, B. Tian, W.Y. Zhang, X.Q. Zhang, Y.Q. Wu, G.X. Lu, Appl. Catal. B: Environ. 204 (2017) 33-42.

Graphical abstract